

Modelling Cycles in Brain Networks with the Hodge Laplacian

Sixtus Dakura, D. Vijay Anand, Zijian Chen, and Moo K. Chung¹

¹University of Wisconsin-Madison, Madison, USA
`vijayanand.4@gmail.com, [sdakurah, zjian.chen, mkchung]@wisc.edu`

Abstract. Cycles or loops in a network embed higher-order interactions beyond pairwise relations. The cycles are essential for the parallel processing of information and enable feedback loops. Despite the fundamental importance of cycles in understanding the higher-order connectivity, identifying and extracting them are computationally prohibitive. This paper proposes a novel persistent homology-based framework for extracting and modelling cycles in brain networks using the Hodge Laplacian. The method is applied in discriminating the functional brain networks of males and females. The code for modeling cycles through the Hodge Laplacian is provided in <https://github.com/laplcebeltrami/hodge>.

Keywords: Topological data analysis · Persistent homology · Hodge Laplacian · Cycles

1 Introduction

The human brain network is a complex system that exhibits collective behaviors at multiple spatial and temporal scales [25]. The mechanisms responsible for these behaviors are often attributed to the higher-order interactions that occur across multiple scales. Understanding the higher-order interactions of the brain regions is crucial to modelling the dynamically evolving structural and functional organization of the brain networks.

The brain networks are often analyzed using graph theory methods that provide quantitative measures ranging from local scales at the node level to global scales at the large community level [4]. Despite the success of graph theory approaches, they can only account for pairwise (dyadic) interactions [2]. The representation of complex networks using high-dimensional objects such as triangles to capture triadic interactions has recently gained traction [2, 11, 19, 22]. The mathematical construct used for this purpose is the simplicial complex, which contains basic building blocks referred to as simplices: nodes (0-simplices), edges (1-simplices), triangles (2-simplices) and tetrahedrons (3-simplices). These simplices systematically encode higher-order interactions [12]. The dynamics of these interactions across multiple scales are quantified by hierarchically generating a nested sequence of simplicial complexes called the filtration in persistent

[†]This study is funded by NIH R01 EB022856, EB02875, NSF MDS-2010778.

homology [10]. In a simplicial complex representation of the brain network, some regions are densely connected while others remain sparse leading to the formation of cycles [21]. A cycle in a brain network is the most fundamental higher-order interaction, which allows for the information flow in a closed path and enables feedback [17, 21]. However, it is not trivial to extract or explicitly model them [5, 9, 10].

This paper aims to model the cyclic relationship in brain networks using the Hodge Laplacian. Further, we develop a new topological inference procedure to characterize cycles across subjects and determine the most discriminating cycles between groups. The explicit cycle modelling framework we introduced allows us to localize the connections contributing to this difference, a novelty not attainable by existing persistent homology methods [7, 10, 16, 20]. The method is applied in determining the most discriminating cycles between the male and female brain networks obtained from the resting-state functional magnetic resonance images (fMRI).

2 Methods

2.1 Homology of a simplicial complex

A k -simplex $\sigma_k = (v_0, \dots, v_k)$ is a k -dimensional convex hull (polytope) of nodes v_0, \dots, v_k . A simplicial complex K is a set of simplices such that for any $\tau_i, \tau_j \in K$, $\tau_i \cap \tau_j$ is a face of both simplices; and a face of any simplex $\tau_i \in K$ is also a simplex in K [10]. A 0-skeleton is a simplicial complex consisting of only nodes. A 1-skeleton is a simplicial complex consisting of nodes and edges. Graphs are 1-skeletons. A k -chain is a finite sum $\sum a_i \tau_i$, where the a_i are either 0 or 1. The set of k -chains forms a group and a sequence of these groups is called a chain complex. To relate different chain groups, we use the boundary maps [24]. For two successive chain groups \mathcal{K}_k and \mathcal{K}_{k-1} , the boundary operator $\partial_k : \mathcal{K}_k \rightarrow \mathcal{K}_{k-1}$ for each k -simplex σ_k is given by

$$\partial_k(\sigma_k) = \sum_{i=0}^k (-1)^i (v_0, \dots, \hat{v}_i, \dots, v_k),$$

where $(v_0, \dots, \hat{v}_i, \dots, v_k)$ gives the $k-1$ faces of σ_k obtained by deleting node \hat{v}_i . The matrix representation $\mathbb{B}_k = (\mathbb{B}_k^{ij})$ of the boundary operator is given by

$$\mathbb{B}_k^{ij} = \begin{cases} 1, & \text{if } \sigma_{k-1}^i \subset \sigma_k^j \text{ and } \sigma_{k-1}^i \sim \sigma_k^j \\ -1, & \text{if } \sigma_{k-1}^i \subset \sigma_k^j \text{ and } \sigma_{k-1}^i \not\sim \sigma_k^j, \\ 0, & \text{if } \sigma_{k-1}^i \not\subset \sigma_k^j \end{cases}, \quad (1)$$

where \sim and $\not\sim$ denote similar and dissimilar orientations respectively.

The kernel of the boundary operator is denoted as $\mathcal{Z}_k = \ker(\partial_k)$ and its image denoted as $\mathcal{B}_k = \text{img}(\partial_{k+1})$. \mathcal{Z}_k and \mathcal{B}_k are the subspaces of \mathcal{K}_k . The elements of \mathcal{Z}_k and \mathcal{B}_k are known as k -cycles and k -boundaries respectively [14]. Note

that $\mathcal{B}_k \subseteq \mathcal{Z}_k$. The set quotient $\mathcal{H}_k = \mathcal{Z}_k/\mathcal{B}_k$ is termed as the k -th homology group [6, 14, 24]. The k -th Betti number $\beta_k = \text{rank}(\mathcal{H}_k)$ counts the number of algebraically independent k -cycles. The first homology group is $\mathcal{H}_1 = \ker(\partial_1)$ since $\text{img}(\partial_2) = \emptyset$.

2.2 Spectral representation of 1-cycles

Hodge Laplacian The Hodge Laplacian \mathcal{L}_k is a higher dimensional generalization of the graph Laplacian for k -simplices [16]. The k -th Hodge Laplacian \mathcal{L}_k is defined as

$$\mathcal{L}_k = \mathbb{B}_{k+1}\mathbb{B}_{k+1}^\top + \mathbb{B}_k^\top\mathbb{B}_k. \quad (2)$$

The k -th homology group \mathcal{H}_k is the kernel of Hodge Laplacian, i.e., $\mathcal{H}_k = \ker\mathcal{L}_k$ [16]. The kernel space of \mathcal{L}_k is spanned by the eigenvectors corresponding to the zero eigenvalues of \mathcal{L}_k . The multiplicity of the zero eigenvalues is β_k . The eigen decomposition of \mathcal{L}_k is given by

$$\mathcal{L}_k \mathbf{U}_k = \mathbf{U}_k \Lambda_k, \quad (3)$$

where Λ_k is the diagonal matrix consisting of eigenvalues of \mathcal{L}_k with corresponding eigenvectors in the columns of \mathbf{U}_k . Brain networks are usually represented as connectivity matrices, from which the 1-skeleton can be obtained by thresholding. For 1-skeletons, the boundary matrix $\mathbb{B}_2 = 0$ and the Hodge Laplacian is reduced to $\mathcal{L}_1 = \mathbb{B}_1^\top\mathbb{B}_1$ [16].

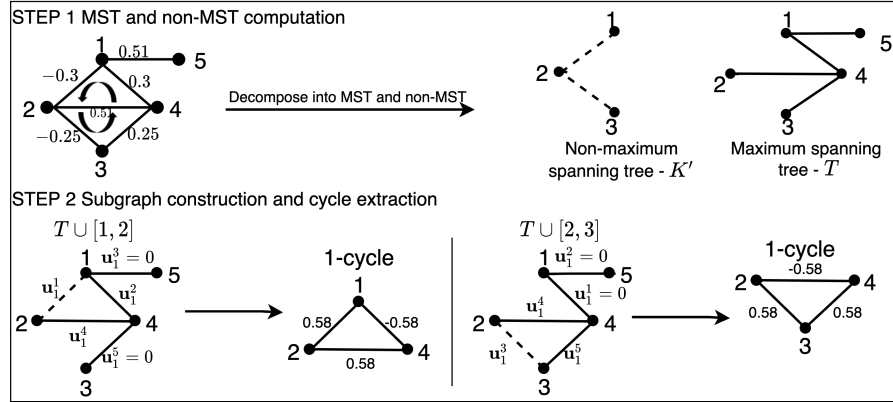


Fig. 1. Construction of 1-cycle basis. STEP 1: A graph is decomposed into MST (T) and non-MST (K'). STEP 2: The subgraphs are formed by adding an edge in K' to T (dotted lines). $\ker\mathcal{L}_1$ for each subgraph is computed to extract a 1-cycle.

Basis representation of cycles We partition the edges of a graph into the maximum spanning tree (MST) (T) and non-MST parts (K') (Figure 1) [23]. If

the m -th edge σ_1^m in K' is added to T , a subgraph

$$\mathcal{X}_m = \{T \cup \sigma_1^m : \sigma_1^m \in K'\}$$

with exactly one 1-cycle is formed. The Hodge Laplacian on \mathcal{X}_m will yield the eigen decomposition identifying the 1-cycle. The entries of the corresponding eigenvector will have non-zero values only for those edges that constitute the cycle and the rest of entries are zero. The m -th 1-cycle is given by

$$\mathcal{C}_m = \sum_{j=1}^{|\mathcal{K}_1|} c_m^j, \quad \text{where} \quad c_m^j = \begin{cases} u_m^j \sigma_1^j, & \text{if } \sigma_1^j \in \mathcal{X}_m \\ 0, & \text{otherwise} \end{cases}. \quad (4)$$

Here, u_m^j is the j -th entry of the m -th eigenvector (a column of \mathbf{U}_1) corresponding to zero eigenvalue. We can show that \mathcal{C}_m forms a basis [1].

Theorem 1. $1\text{-cycles } \mathcal{C}_1, \dots, \mathcal{C}_{|K'|}$ spans $\ker \mathcal{L}_1$ and forms a basis over the collection of all possible 1-cycles.

Proof. Let E_m be the edge set of the cycle \mathcal{C}_m . Since E_m and E_n differ at least by two edges, they are algebraically independent. Hence, all the cycles $\mathcal{C}_1, \dots, \mathcal{C}_{|K'|}$ are linearly independent from each other. Since there should be exactly $\beta_1 = |K'|$ number of independent cycles in the 1-st Homology group $H_1 = \ker \mathcal{L}_1$, $\{\mathcal{C}_1, \dots, \mathcal{C}_{|K'|}\}$ spans $\ker \mathcal{L}_1$.

Example 1. We illustrate how to compute the 1-cycle basis. Consider the subgraph $T \cup [1, 2]$ in Figure 1. The boundary matrix \mathbb{B}_1 and the corresponding Hodge Laplacian \mathcal{L}_1 is computed as

$$\mathbb{B}_1 = \begin{bmatrix} [1, 2] & [1, 4] & [1, 5] & [2, 4] & [3, 4] \\ [1] & 1 & 1 & 0 & 0 \\ [2] & -1 & 0 & 0 & 1 & 0 \\ [3] & 0 & 0 & 0 & 0 & 1 \\ [4] & 0 & -1 & 0 & -1 & -1 \\ [5] & 0 & 0 & -1 & 0 & 0 \end{bmatrix} \quad \mathcal{L}_1 = \mathbb{B}_1^T \mathbb{B}_1 = \begin{pmatrix} 2 & 1 & 1 & -1 & 0 \\ 1 & 2 & 1 & 1 & 1 \\ 1 & 1 & 2 & 0 & 0 \\ -1 & 1 & 0 & 2 & 1 \\ 0 & 1 & 0 & 1 & 2 \end{pmatrix}.$$

The eigen decomposition $\mathcal{L}_1 \mathbf{U}_1 = \mathbf{U}_1 \Lambda_1$ is given by

$$\mathbf{U}_1 = \begin{bmatrix} \mathbf{u}_1 & \mathbf{u}_2 & \mathbf{u}_3 & \mathbf{u}_4 & \mathbf{u}_5 \\ [1, 2] & \mathbf{0.58} & -0.25 & 0.37 & -0.60 & 0.33 \\ [1, 4] & -\mathbf{0.58} & -0.49 & 0.00 & 0.00 & 0.65 \\ [1, 5] & \mathbf{0.00} & 0.57 & -0.60 & -0.37 & 0.42 \\ [2, 4] & \mathbf{0.58} & -0.25 & -0.37 & 0.60 & 0.22 \\ [3, 4] & \mathbf{0.00} & 0.57 & 0.60 & 0.37 & 0.43 \end{bmatrix} \quad \Lambda_1 = \begin{pmatrix} \mathbf{0.00} & 0 & 0 & 0 & 0 \\ 0 & 0.70 & 0 & 0 & 0 \\ 0 & 0 & 1.38 & 0 & 0 \\ 0 & 0 & 0 & 3.62 & 0 \\ 0 & 0 & 0 & 0 & 4.30 \end{pmatrix}.$$

The 1-cycle is then represented as

$$\mathcal{C}_1 = 0.58\sigma_1^1 - 0.58\sigma_1^2 + 0.00\sigma_1^3 + 0.00\sigma_1^4 + 0.58\sigma_1^5 + 0.00\sigma_1^6,$$

where $\sigma_1^1 = [1, 2]$, $\sigma_1^2 = [1, 4]$, $\sigma_1^3 = [1, 5]$, $\sigma_1^4 = [2, 3]$, $\sigma_1^5 = [2, 4]$, and $\sigma_1^6 = [3, 4]$. Similarly, the cycle in the second subgraph $T \cup [2, 3]$ is represented as

$$\mathcal{C}_2 = 0.00\sigma_1^1 + 0.00\sigma_1^2 + 0.00\sigma_1^3 + 0.58\sigma_1^4 - 0.58\sigma_1^5 + 0.58\sigma_1^6.$$

Any cycle in the graph \mathcal{X} can be represented as a linear combination of basis \mathcal{C}_1 and \mathcal{C}_2 . For large graphs, the coefficients of basis expansion can be vectorized and efficiently stored as a sparse matrix.

2.3 Common 1-cycles across networks

Using the 1-cycle basis, we identify common 1-cycles across different networks. We extend the idea of extracting 1-cycle basis for a single network (individual level) to collection of networks (group level). Let $\bar{\mathcal{S}} = (\bar{\mathcal{S}}_{i,j})$ be the average of all the individual connectivity matrices. $\bar{\mathcal{S}}$ is used to construct a graph $\bar{\mathcal{X}}$ where we assume any two nodes (i, j) in $\bar{\mathcal{X}}$ is incident by an edge if $\bar{\mathcal{S}}_{i,j} > 0$, i.e., positive correlations [3, 18, 30]. The cycles extracted from $\bar{\mathcal{X}}$ will represent the common cycle basis. To reflect the individual network variability, we model the vectorized individual network connectivity \mathcal{M} as a linear combination of the common 1-cycle basis. This gives the minimization problem

$$\arg \min_{\boldsymbol{\alpha}} \|\mathcal{M} - \boldsymbol{\psi}\boldsymbol{\alpha}\|_2^2, \quad (5)$$

where the basis matrix $\boldsymbol{\psi} = [\mathcal{C}_1, \dots, \mathcal{C}_{|K'|}]$, and \mathcal{C}_m 's are the 1-cycle basis from $\bar{\mathcal{X}}$. The coefficients vector $\boldsymbol{\alpha} = [\alpha_1, \dots, \alpha_{|K'|}]^\top$ is estimated in the least squares fashion as $\hat{\boldsymbol{\alpha}} = (\boldsymbol{\psi}^\top \boldsymbol{\psi})^{-1} \boldsymbol{\psi}^\top \mathcal{M}$.

Let $\bar{\alpha}_m^1$ and $\bar{\alpha}_m^2$ be the mean coefficients corresponding to the m -th 1-cycle basis of networks in group \mathcal{N}_1 and \mathcal{N}_2 respectively. We propose the following statistic for testing the group difference [1]:

$$\mathcal{T}(\mathcal{N}_1, \mathcal{N}_2) = \max_{1 \leq m \leq |K'|} |\bar{\alpha}_m^1 - \bar{\alpha}_m^2|. \quad (6)$$

The statistical significance is determined using the permutation test [8].

3 Validation

The proposed methodology is validated on network simulations with different number of cycles. The simulation is done using deltoid, limacon trisectrix and trifolium [29]. Groups 1 and 2 have three 1-cycles each and are topologically equivalent. Groups 3 and 4 have five 1-cycles each and are topologically equivalent. 50 points were sampled along these curves and perturbed with noise $N(0, 0.025^2)$. 10 networks were generated in each group. All the networks consists of identical number of nodes. For networks with different number of nodes, data augmentation can be done [23]. The simulation code is provided in <https://github.com/laplcebeltrami/hodge>.

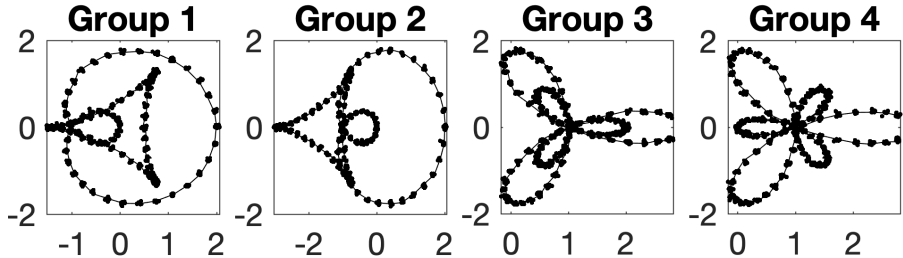


Fig. 2. Random networks used in Validation. Groups 1 and 2 have three 1-cycles and topologically equivalent. Groups 3 and 4 have five 1-cycles and topologically equivalent.

We validated whether the test statistic (6) can discriminate networks with different topology. 10,000 permutations were used to compute the p-values. Since there are no established methods for modeling cycles, we validated our method against geometric distances \mathcal{L}_1 , \mathcal{L}_2 , \mathcal{L}_∞ and the Gromov-Hausdorff (GH) distance [8]. The simulations were performed 50 times and the results are given in Table 1, where the average p-values are reported. Also, we reported the false positive rates computed as the fraction of 50 simulations with p-values below 0.05 and the false negative rates computed as the fraction of 50 simulations with p-values above 0.05 [23].

We tested if the proposed method can detect *topological equivalence* by comparing Groups 1 vs. 1, 2 vs. 2, 1 vs. 2, 3 vs. 3, 4 vs. 4 and 3 vs. 4 (first 6 rows). The test procedures should not detect signals and higher p-values and smaller false positive rates are preferred. The proposed method \mathcal{T} performed well compared to the other distances. We also tested if the proposed method can detect *topological difference* by comparing Groups 1 vs. 3, 1 vs. 4, 2 vs. 3 and 2 vs. 4. The test procedures should detect signals and smaller p-values and smaller false negative rates are preferred. \mathcal{T} consistently outperformed the other distances.

This study shows that existing methods will likely produce significant topological false negatives while reasonably good at not producing large false positives. However, the proposed method will not produce large amount of topological false positives and negatives at the same time.

4 Application

Dataset We used a subset of the resting-state fMRI (rs-fMRI) data in the Human Connectome Project [28, 27]. rs-fMRI are collected at 2 mm isotropic voxels and 1200 time points [27]. Data that went through the standard minimal pre-processing pipelines [13] was used. Volumes with framewise displacement larger than 0.5mm and their neighbors were scrubbed [28, 27]. Twelve subjects having excessive head movement were excluded from the dataset. Subsequently, the Automated Anatomical Labeling (AAL) template is used to parcellate and average rs-fMRI spatially into 116 non-overlapping anatomical regions [26]. The details

Table 1. The performance results showing average p-values, false positive rates (first 6 rows) and false negative rates (last 4 rows). Group 1 and 2 have three 1-cycles and topologically equivalent. Group 3 and 4 have five 1-cycles and topologically equivalent. Smaller false positive and false negative rates are preferred.

Groups	\mathcal{L}_1	\mathcal{L}_2	\mathcal{L}_∞	GH	\mathcal{T}
1 vs. 1	0.26 ± 0.15 (0.04)	0.27 ± 0.14 (0.04)	0.24 ± 0.13 (0.00)	0.45 ± 0.31 (0.12)	0.60 ± 0.26 (0.00)
2 vs. 2	0.29 ± 0.14 (0.04)	0.31 ± 0.15 (0.00)	0.26 ± 0.14 (0.12)	0.56 ± 0.25 (0.04)	0.53 ± 0.29 (0.04)
1 vs. 2	0.27 ± 0.15 (0.08)	0.25 ± 0.15 (0.08)	0.20 ± 0.12 (0.12)	0.43 ± 0.24 (0.04)	0.38 ± 0.28 (0.16)
3 vs. 3	0.28 ± 0.16 (0.08)	0.27 ± 0.15 (0.04)	0.23 ± 0.15 (0.04)	0.45 ± 0.25 (0.00)	0.52 ± 0.31 (0.08)
3 vs. 4	0.23 ± 0.14 (0.18)	0.23 ± 0.14 (0.12)	0.26 ± 0.13 (0.18)	0.52 ± 0.27 (0.04)	0.52 ± 0.30 (0.03)
4 vs. 4	0.32 ± 0.15 (0.04)	0.30 ± 0.15 (0.04)	0.24 ± 0.14 (0.16)	0.49 ± 0.28 (0.10)	0.41 ± 0.28 (0.04)
1 vs. 3	0.26 ± 0.14 (0.92)	0.25 ± 0.14 (0.88)	0.27 ± 0.13 (0.88)	0.00 ± 0.00 (0.00)	0.00 ± 0.00 (0.00)
1 vs. 4	0.29 ± 0.14 (0.72)	0.28 ± 0.16 (0.80)	0.27 ± 0.16 (0.72)	0.00 ± 0.00 (0.00)	0.00 ± 0.00 (0.00)
2 vs. 3	0.25 ± 0.17 (0.76)	0.24 ± 0.17 (0.76)	0.25 ± 0.15 (0.88)	0.00 ± 0.00 (0.00)	0.00 ± 0.00 (0.00)
2 vs. 4	0.27 ± 0.15 (0.88)	0.23 ± 0.15 (0.80)	0.22 ± 0.14 (0.96)	0.00 ± 0.00 (0.00)	0.00 ± 0.00 (0.00)

on image processing is given in [15]. The final data is comprised of the fMRI of 400 subjects of which 168 are males and 232 are females.

Sexual dimorphism in 1-cycles We constructed the network template by averaging 400 subjects connectivity matrices. The 1-cycle basis was then extracted from this network template. The average network template contains $p = 116$ nodes, hence we expect $q = p(p-1)/2 = 6555$ linearly independent 1-cycles [23]. Each individual connectivity matrix is then expanded and the test carried out using the estimated expansion coefficients resulting in the observed test statistic of 0.41. 0.1 million permutations were used to obtain the p-value of 0.03. We compared the discriminating power of our method against geometric distances \mathcal{L}_1 , \mathcal{L}_2 , \mathcal{L}_∞ and GH distance, which respectively give the p-values of 0.014, 0.004, 0.013, 0.54. All the baseline methods performed well except for the GH distance. Nonetheless, only the statistic \mathcal{T} can localize the connections contributing to the difference. Figure 3-top shows the four most discriminating cycles. The edge color represents the average correlation difference between the groups.

Sexual dimorphism in 0-cycles Our method for 1-cycles is also applicable to 0-cycles (connected components) by replacing Hodge Laplacian \mathcal{L}_1 with graph

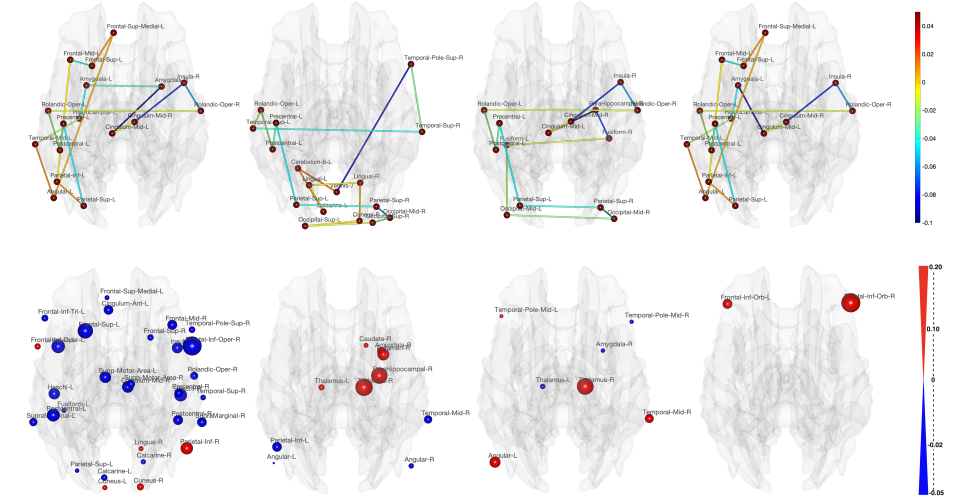


Fig. 3. Top: The four most discriminating cycles corresponding to maximum test statistic values. The edge colors correspond to the edge weight differences (female - male). Bottom: The four most discriminating connected components. The size of nodes correspond to the weighted node degree differences (female - male).

Laplacian \mathcal{L}_0 . The basis will be defined along nodes. The j -th basis vector will have value 1 at node j and 0 in other places. Including the test statistic, the same pipeline can be used. Since no data is defined on nodes, we used the weighted degree (sum of correlations of all the edges connecting at each node). The observed test statistic is 27.41, which gives the p-value of 0.006. Figure 3-bottom shows the four most discriminating 0-cycles. The node size corresponds to the difference (female - male) in the weighted degree between the groups.

5 Conclusion

We proposed a novel Hodge Laplacian framework for explicitly identifying and modelling cycles in brain networks. We were able to show that cycles, both 0- and 1-cycles are topologically significant features in discriminating between males and females. The four most discriminating 1-cycles include the inferior parietal lobule (Parietal-Inf-L), the rolandic operculum (Rolandic-Oper-L, Rolandic-Oper-R), and the amygdala (Amygdala-R, Amygdala-L) (Figure 3-top). The symmetric connections between the left and right rolandic operculum, superior parietal lobule as well as the middle cingulate are consistently showing up in at least 2 most dominating cycles. The most discriminating 0-cycles (Figure 3-bottom) also contain most of these brain regions. The method can be extended to higher order connectivity such as 2-cycles using higher order Hodge Laplacians. This is left as a future study.

References

1. Anand, D.V., Dakurah, S., Wang, B., Chung, M.K.: Hodge-laplacian of brain networks and its application to modeling cycles. arXiv preprint arXiv:2110.14599 (2021)
2. Battiston, F., Cencetti, G., Iacopini, I., Latora, V., Lucas, M., Patania, A., Young, J.G., Petri, G.: Networks beyond pairwise interactions: structure and dynamics. Physics Reports **874**, 1–92 (2020)
3. Buckner, R.L., Sepulcre, J., Talukdar, T., Krienen, F.M., Liu, H., Hedden, T., Andrews-Hanna, J.R., Sperling, R.A., Johnson, K.A.: Cortical hubs revealed by intrinsic functional connectivity: mapping, assessment of stability, and relation to alzheimer’s disease. Journal of neuroscience **29**, 1860–1873 (2009)
4. Bullmore, E., Sporns, O.: Complex brain networks: graph theoretical analysis of structural and functional systems. Nature reviews neuroscience **10**, 186–198 (2009)
5. Busaryev, O., Cabello, S., Chen, C., Dey, T.K., Wang, Y.: Annotating simplices with a homology basis and its applications. In: Scandinavian workshop on algorithm theory. pp. 189–200. Springer (2012)
6. Chen, C., Freedman, D.: Measuring and computing natural generators for homology groups. Computational Geometry **43**, 169–181 (2010)
7. Chung, M.K., Huang, S.G., Songdechakraiut, T., Carroll, I.C., Goldsmith, H.H.: Statistical analysis of dynamic functional brain networks in twins. arXiv preprint arXiv:1911.02731 (2019)
8. Chung, M.K., Lee, H., DiChristofano, A., Ombao, H., Solo, V.: Exact topological inference of the resting-state brain networks in twins. Network Neuroscience **3**, 674–694 (2019)
9. Dey, T.K., Fan, F., Wang, Y.: Computing topological persistence for simplicial maps. In: Proceedings of the thirtieth annual symposium on Computational geometry. pp. 345–354 (2014)
10. Edelsbrunner, H., Harer, J., et al.: Persistent homology-a survey. Contemporary mathematics **453**, 257–282 (2008)
11. Farazi, M., Zhan, L., Lepore, N., Thompson, P.M., Wang, Y.: A univariate persistent brain network feature based on the aggregated cost of cycles from the nested filtration networks. In: 2020 IEEE 17th International Symposium on Biomedical Imaging (ISBI). pp. 1–5. IEEE (2020)
12. Giusti, C., Ghrist, R., Bassett, D.S.: Two’s company, three (or more) is a simplex. Journal of computational neuroscience **41**, 1–14 (2016)
13. Glasser, M.F., Sotiropoulos, S.N., Wilson, J.A., Coalson, T.S., Fischl, B., Andersson, J.L., Xu, J., Jbabdi, S., Webster, M., Polimeni, J.R., et al.: The minimal preprocessing pipelines for the human connectome project. Neuroimage **80**, 105–124 (2013)
14. Hatcher, A., Press, C.U., of Mathematics, C.U.D.: Algebraic Topology. Algebraic Topology, Cambridge University Press (2002)
15. Huang, S.G., Samdin, S.B., Ting, C.M., Ombao, H., Chung, M.K.: Statistical model for dynamically-changing correlation matrices with application to brain connectivity. Journal of neuroscience methods **331**, 108480 (2020)
16. Lee, H., Chung, M.K., Kang, H., Lee, D.S.: Hole detection in metabolic connectivity of alzheimer’s disease using k-laplacian. In: International Conference on Medical Image Computing and Computer-Assisted Intervention. pp. 297–304. Springer (2014)

17. Lind, P.G., Gonzalez, M.C., Herrmann, H.J.: Cycles and clustering in bipartite networks. *Physical Review E* **72**, 056127 (2005)
18. Meunier, D., Lambiotte, R., Fornito, A., Ersche, K., Bullmore, E.T.: Hierarchical modularity in human brain functional networks. *Frontiers in neuroinformatics* **3**, 37 (2009)
19. Petri, G., Expert, P., Turkheimer, F., Carhart Harris, R., Nutt, D., Hellyer, P.J., Vaccarino, F.: Homological scaffolds of brain functional networks. *Journal of The Royal Society Interface* **11**, 20140873 (2014)
20. Reami, Y., Bobrowski, O.: Cycle registration in persistent homology with applications in topological bootstrap. arXiv preprint arXiv:2101.00698 (2021)
21. Sizemore, A.E., Giusti, C., Kahn, A., Vettel, J.M., Betzel, R.F., Bassett, D.S.: Cliques and cavities in the human connectome. *Journal of computational neuroscience* **44**, 115–145 (2018)
22. Sizemore, A.E., Phillips Cremins, J.E., Ghrist, R., Bassett, D.S.: The importance of the whole: topological data analysis for the network neuroscientist. *Network Neuroscience* **3**, 656–673 (2019)
23. Songdechakraiut, T., Shen, L., Chung, M.: Topological learning and its application to multimodal brain network integration. In: International Conference on Medical Image Computing and Computer-Assisted Intervention. pp. 166–176. Springer (2021)
24. Topaz, C.M., Ziegelmeier, L., Halverson, T.: Topological data analysis of biological aggregation models. *PloS one* **10**, e0126383 (2015)
25. Torres, L., Blevins, A.S., Bassett, D., Eliassi-Rad, T.: The why, how, and when of representations for complex systems. *SIAM Review* **63**, 435–485 (2021)
26. Tzourio-Mazoyer, N., Landeau, B., Papathanassiou, D., Crivello, F., Etard, O., Delcroix, N., Mazoyer, B., Joliot, M.: Automated anatomical labeling of activations in spm using a macroscopic anatomical parcellation of the mni mri single-subject brain. *Neuroimage* **15**, 273–289 (2002)
27. Van Essen, D.C., Smith, S.M., Barch, D.M., Behrens, T.E., Yacoub, E., Ugurbil, K., Consortium, W.M.H., et al.: The wu-minn human connectome project: an overview. *Neuroimage* **80**, 62–79 (2013)
28. Van Essen, D.C., Ugurbil, K., Auerbach, E., Barch, D., Behrens, T.E., Bucholz, R., Chang, A., Chen, L., Corbetta, M., Curtiss, S.W., et al.: The human connectome project: a data acquisition perspective. *Neuroimage* **62**, 2222–2231 (2012)
29. Yates, R.C.: Curves and their properties. (1974)
30. Zhan, L., Jenkins, L.M., Wolfson, O.E., GadElkarim, J.J., Nocito, K., Thompson, P.M., Ajilore, O.A., Chung, M.K., Leow, A.D.: The significance of negative correlations in brain connectivity. *Journal of Comparative Neurology* **525**, 3251–3265 (2017)